

Probing universal imaginary-time relaxation critical dynamics with infinite projected entangled pair states

He-Yu Lin,^{1,2,3} Shuai Yin,^{4,5} Z. Y. Xie,^{1,2,*} and Zhong-Yi Lu^{1,2,†}

¹*Department of Physics, Renmin University of China, Beijing 100872, China*

²*Key Laboratory of Quantum State Construction and Manipulation (Ministry of Education), Renmin University of China, Beijing, 100872, China*

³*School of Science, Inner Mongolia University of Science and Technology, Baotou 014010, China*

⁴*Guangdong Provincial Key Laboratory of Magnetoelectric Physics and Devices, Sun Yat-Sen University, Guangzhou, 510275, China*

⁵*School of Physics, Sun Yat-Sen University, Guangzhou, 510275, China*

(Dated: November 17, 2025)

We investigate the imaginary-time relaxation critical dynamics of the two-dimensional transverse-field Ising model using infinite projected entangled pair states (iPEPS) with the full-update strategy. Simulating directly in the thermodynamic limit, we explore the relaxation process near the critical point with two types of initial states: a fully polarized state and a product state with a small magnetization. For the fully polarized state, the magnetization shows a power law scaling $M \propto \tau^{-\beta/(\nu z)}$ in the imaginary-time evolution, from which both the critical point and critical exponent can be determined with high accuracy. For the nearly paramagnetic state, the relaxation process exhibits a behavior of $M \propto \tau^\theta$ with $\theta = 0.1958$ being the critical initial-slip exponent, which is in good agreement with that obtained from the dynamic scaling of the self-correlation in quantum Monte Carlo method. These universal features emerge well before the system converges to the ground state, demonstrating the efficiency of imaginary-time evolution for probing quantum criticality. Our results demonstrate that iPEPS can serve as a robust and scalable method for studying dynamical critical phenomena in two-dimensional quantum many-body systems.

I. INTRODUCTION

Understanding nonequilibrium critical dynamics is a central issue in statistical mechanics and condensed matter physics. Among various realizations of nonequilibrium processes, imaginary-time evolution has emerged as a robust framework that not only works as a routine method to determine the ground state of quantum many-body systems [1–4] but also encodes universal information in its transient stages [5]. Moreover, the study of imaginary-time dynamics is heating up due to recent advances in quantum computers [6, 7].

Near quantum critical points, the imaginary-time evolution of a quantum system can exhibit universal scaling behaviors incorporating the equilibrium critical information of the quantum phase transitions and the intrinsic nonequilibrium scaling properties [8–11], and provides an analogy to the short-time critical dynamics in classical critical points [12–15]. This makes the imaginary-time evolution especially suitable for probing critical properties in strongly correlated systems [8, 16, 17]. A remarkable advantage of this method is that the computational cost can be significantly reduced, since universal critical properties can be reliably extracted during the short-time stage of the evolution process [8, 13]. Recently, this method has even shown its power in sign-problematic fermionic models in quantum Monte Carlo simulations

[18, 19]. In addition, the scaling theory of the imaginary-time relaxation critical dynamics has been verified in programmable quantum circuits [20].

A series of numerical methods have been developed to study the critical properties of the strongly correlated many-body systems [21]. Among these efforts, tensor network states combined with the renormalization group techniques [22] are free of sign problems, can deal with the infinite quantum systems satisfying the area law of the entanglement entropy [23], and thus are drawing increasing attentions in studying quantum magnetization [24–28], superconductivity [3, 29], topological order [30–32], quantum field theory [33, 34], and so on. Imaginary-time evolution of tensor network states is well-established [1, 2, 4]. While it is extensively used in studying the ground state and thermodynamics, it is seldom employed to study the critical dynamics in a nonequilibrium system.

In this work, we employ the infinite projected entangled pair state (iPEPS) [35], a member of the tensor network family, to study the imaginary-time dynamics of the two-dimensional transverse-field Ising model (TFIM). Specifically, adopting the full-update strategy [36–38], we calculate the magnetization M as a function of the inverse temperature τ during the imaginary-time evolution of two distinct states respectively as an initial state: a fully polarized ferromagnetic state and a product state with a tiny magnetization. For the former case, we confirm the scaling behavior $M(\tau) \sim \tau^{-\beta/(\nu z)}$, where β and ν are the critical exponents corresponding to the order parameter and correlation length, respectively, and z is the dynamical critical exponent. It shows that even with

* qingtaoxie@ruc.edu.cn

† zlu@ruc.edu.cn

moderate bond dimensions, this scaling relation provides an efficient estimator for both the critical point and the associated critical exponents. For the latter case, we find that the short-time dynamics exhibits a critical initial-slip behavior, for which $M \propto \tau^\theta$ with θ being the critical initial-slip exponent. In addition, we show that the exponent θ can systematically approach the value obtained from the quantum Monte Carlo method as the bond dimension increases, demonstrating that iPEPS can reliably capture universal early-time dynamics.

This work highlights the power of iPEPS with imaginary-time evolution for probing dynamical critical behavior in two-dimensional quantum systems. The method is not only free of the sign problem and finite-size limitations, but also leverages the fact that universal properties can emerge before the system converges to the ground state. This makes it a versatile and efficient approach for investigating quantum criticality, and a promising strategy for future studies of more complex models such as frustrated magnets and interacting fermionic systems.

The rest of the paper is organized as follows. Sec. II gives a brief review on the scaling theory of the imaginary-time relaxation dynamics. After introducing the two-dimensional TFIM and the iPEPS method used in this work in Sec. III, we then present the obtained result of the relaxation dynamics in detail in Sec. IV. Finally, we summarize and conclude in Sec. V.

II. SCALING THEORY OF QUANTUM CRITICAL RELAXATION

Starting from an initial state $|\psi_0\rangle$, the evolving quantum state $|\psi(\tau)\rangle$ governed by Hamiltonian H at imaginary time τ is given by

$$|\psi(\tau)\rangle = \frac{e^{-\tau H}|\psi_0\rangle}{\|e^{-\tau H}|\psi_0\rangle\|}, \quad (1)$$

For a system with an energy gap Δ , when $\tau \gg \Delta^{-1}$, $|\psi(\tau)\rangle$ can converge to the ground state as long as $|\psi_0\rangle$ has a non-zero overlap with the ground state. Thus, the imaginary-time evolution has been widely used in numerical simulations to determine the ground state of quantum many-body systems. In contrast, at critical points and in the thermodynamic limit, with $\Delta \rightarrow 0$, $|\psi(\tau)\rangle$ can hardly reach the true ground state, and this is known as the critical slowing down.

In analogy to the short-time critical dynamics in classical critical points [12–15], it has been shown that the imaginary-time relaxation dynamics near a quantum critical point can exhibit universal scaling behavior [8, 9]. For an uncorrelated initial state with magnetization M_0 , after some nonuniversal microscopic transient time, the scale transformation of the order parameter M reads [8–10],

$$M(\tau, g, M_0) = b^{-\beta/\nu} M(\tau b^{-z}, g b^{1/\nu}, U(M_0, b)), \quad (2)$$

where b is a rescaling factor, g measures the distance away from criticality, and $U(M_0, b)$ is the universal characteristic function describing the scale transformation of M_0 , which was firstly proposed in classical phase transition [14] and then generalized to quantum criticality [9].

For a tiny M_0 , $U(M_0, b) = M_0 b^{x_0}$ with x_0 being the scaling dimension of M_0 [8, 9, 14]. At the critical point ($g = 0$), choosing $b = \tau^{1/z}$ leads to the scaling form,

$$M(\tau, M_0) = \tau^{-\beta/(\nu z)} f_M(M_0 \tau^{x_0/z}). \quad (3)$$

And then the Taylor expansion of f_M on $M_0 \tau^{x_0/z}$ gives the following scaling relation [8, 9]

$$M(\tau) \sim M_0 \tau^\theta, \quad (4)$$

where

$$\theta = \frac{x_0 - \beta/\nu}{z}. \quad (5)$$

When $\theta > 0$, Eq. (4) indicates that the order parameter grows in the short-time stage. This refers to the critical initial-slip behavior in the imaginary-time direction. In contrast, in the long-time stage with $\tau \gg \tau_{\text{cr}} \sim M_0^{-z/x_0}$, the influence of the initial state fades and the order parameter decays as $M \propto \tau^{-\beta/(\nu z)}$.

For a saturated M_0 , $U(M_0, b)$ is a constant since the fully polarized state corresponds to a renormalization fixed point of the system. Thus, in this case, at the critical point with $g = 0$, $M(\tau)$ decays as [8, 9]

$$M(\tau) \propto \tau^{-\beta/(\nu z)}, \quad (6)$$

after a transient time scale.

III. MODEL AND METHOD

The transverse-field Ising model (TFIM) [39–41] on a square lattice serves as a prototypical model for investigating quantum phase transitions [40, 42, 43] and critical dynamics [44] in quantum many-body systems. Its Hamiltonian is given by

$$H = -J \sum_{\langle i, j \rangle} \sigma_i^z \sigma_j^z - h \sum_i \sigma_i^x, \quad (7)$$

where σ_i^x and σ_i^z are Pauli matrices defined on site i , J denotes the nearest-neighbor ferromagnetic coupling, and h is the transverse field. We set $J = 1$ in this work.

At zero temperature, the system undergoes a quantum phase transition at a critical field $h_c \approx 3.044$ [40, 41, 45], separating a ferromagnetic phase with spontaneous magnetization in z -direction ($h < h_c$) from a quantum paramagnetic phase ($h > h_c$) [39, 46]. The order parameter characterizing this phase transition is defined as $M = \langle \sigma_z \rangle$. Due to the quantum-to-classical mapping between a d -dimensional quantum system and a $(d+1)$ -dimensional classical statistical model [42, 46, 47], the

transition belongs to the three-dimensional classical Ising universality class, where the order parameter exponent $\beta \approx 0.3264$, the correlation length exponent $\nu \approx 0.62997$, and the dynamic exponent $z = 1$, yielding a short-time exponent $-\beta/(\nu z) \approx -0.518$. In addition, the critical initial-slip exponent θ has been previously estimated as $\theta \approx 0.209(4)$ by the quantum Monte Carlo method [10].

In this work, we use the two-dimensional tensor-network method to simulate the imaginary-time relaxation dynamics of TFIM represented by Eq. (7). Employing the translation symmetry of a Hamiltonian system, e.g., the TFIM, the tensor network states can offer a faithful representation of any quantum state satisfying the area law with parameters with only polynomial growth in number. Being free of sign problems, in recent years tensor network states have been utilized successfully to study the ground state of strongly correlated systems near quantum critical points [24, 27, 28, 48], low-lying excitations and dynamical correlation functions [49, 50], thermodynamics [51, 52], and also real-time dynamics [53, 54].

In this work, we choose the most popular tensor network state, i.e., the iPEPS ansatz, to represent the imaginary-time-evolving quantum states. Specifically, for TFIM on a square lattice in this work, the iPEPS wave function is written as

$$|\Psi\rangle = \sum_{\{\sigma\}} \left[\text{Tr} \prod_i T_{l_i r_i u_i d_i \sigma_i}^{(i)} \right] |\sigma_1 \sigma_2 \dots \sigma_i \dots\rangle, \quad (8)$$

where $T^{(i)}$ denotes the local tensor defined on site i , with virtual indices (l_i, r_i, u_i, d_i) connecting to the left, right, up, and down neighbors, and σ_i labeling the local physical spin state. The bond dimension D , which defines the size of each virtual index, provides an upper bound on the entanglement capacity. Generally, a larger D enables a more accurate representation of highly entangled states [36] but leads to a significantly higher cost. For an uncorrelated state, or a product state, $D = 1$ will be sufficient.

For the TFIM represented in Eq. (7), we use a 2×2 unit cell composed of two distinct local tensors which are determined by the imaginary-time evolution [1, 2]. Dividing the imaginary-time τ into many small slices, $\tau = n\delta$, and decomposing the time-evolution operator $e^{-\delta H}$ into a sequence of two-site operators through a Trotter-Suzuki decomposition [47], the time evolution can be performed efficiently by updating the wavefunction successively after evolution of each two-site operator.

To accurately simulate the critical dynamics, in this work we adopted the full-update strategy [36–38] to update the wavefunction during the imaginary-time evolution. In order to perform this strategy, we firstly compute the whole environment of a two-site system using the corner transfer-matrix renormalization group algorithm [3, 55], which approximates the environment with a small tensor network with bond dimension χ , then we determine the two local tensors which construct the ap-

proximated updated wavefunction by minimizing the distance between the wavefunctions before and after the evolution, and finally we update the wavefunction and perform the next two-site time evolution similarly. This process is performed again and again, until the imaginary time τ is reached.

In our calculations, we always keep χ sufficiently large to make the environment accurate. As long as this is done, the minimization problem can be solved efficiently by a linear search or a recursive method [37, 38]. We find that incorporating full environmental information enables the accurate tracking of entanglement growth and correlation spreading, which is crucial for capturing critical dynamics.

IV. RESULTS

In the following, we apply the full-update strategy-assisted iPEPS method to study the imaginary-time relaxation dynamics of the two-dimensional TFIM. We consider two representative initial states, namely a fully polarized ferromagnetic state with magnetization $M_0 = 1$, and a nearly paramagnetic state with a tiny M_0 [8, 9].

A. Relaxation dynamics for a fully polarized state

In this section, we explore the imaginary-time relaxation critical dynamics of model (7) from an initial state with complete polarization, i.e., $M_0 = 1$. For comparison, the imaginary-time evolution is simulated for several (D, χ) setups, with $M(\tau)$ computed for different transverse fields h . The detailed results are summarized in Fig. 1.

As reviewed in Sec. II, at the critical point in this case, the magnetization should exhibit a power behavior $M(\tau) \sim \tau^{-\beta/(\nu z)}$. To guide the eyes, we plot Fig. 1 in a log-log scale. For each (D, χ) calculation, we can determine a h^* which gives the best power behavior of $M(\tau)$ and can be regarded as an estimation of h_c at a fixed (D, χ) . As long as h^* is fixed, the estimated short-time exponent $\beta/(\nu z)$ can be obtained by a power-law fitting at h^* .

As shown in Fig. 1(a), for $D = 3$, $h^* = 3.064$. When $h < h^*$, such as the black and red curves there, the magnetization bends upward, corresponding to the symmetry-breaking phase in z -direction, while when $h > h^*$, such as the green and purple curves there, the magnetization bends downward, corresponding to the paramagnetic phase. This phenomenon means that h^* can be regarded as an unstable fixed point in the renormalization group approximately, and can be used as an estimator of the critical point corresponding to the quantum phase transition. The dashed yellow line in Fig. 1(a) is a power-law fitting of $M(\tau)$ at $h = h^*$, and the slope $k^* = -0.52339$ can be regarded as an estimation of $-\beta/(\nu z)$.

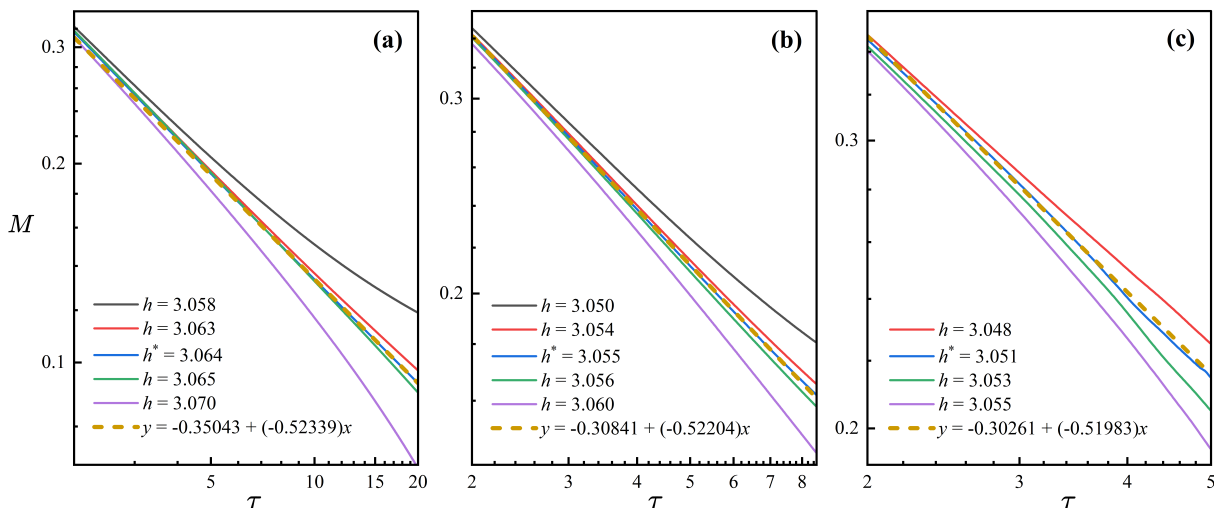


FIG. 1: Imaginary-time relaxation dynamics for a fully polarized initial state, plotted in log-log scale. Magnetization $M(\tau)$ obtained from iPEPS with different bond dimensions (D) and environment bond dimensions (χ) is summarized together. In each calculation, the transverse field leading to the best linear curve is denoted as h^* , and for each h^* , a linear fitting is performed and is denoted as dashed yellow. (a) For $D = 3$ and $\chi = 30$. (b) For $D = 4$ and $\chi = 60$. (c) For $D = 5$ and $\chi = 60$.

Things are similar for $D = 4$ in Fig. 1(b) and $D = 5$ in Fig. 1(c). The only difference lies in the fact that with a different bond dimension D , we obtain slightly different h^* and k . To be specific, for $D = 4$ we obtain $h^* = 3.055$ and $k^* = -0.52204$, and for $D = 5$, we have $h^* = 3.051$ and $k^* = -0.51983$.

For tensor network states, it is widely known that D controls the number of variational parameters and the upper bound of the encoded entanglement entropy; therefore, it is generally believed that the larger D is, the more accurate the iPEPS representation and thus the related calculations are. This is indeed consistent with our calculations. As mentioned in Sec. III, the critical transverse field h_c was estimated as about 3.044 in previous calculations [40, 41, 45], which is closer to the result obtained in $D = 5$. Actually, in order to further eliminate the finite D effect, in Fig. 2, we plot h^* as a function of $1/D$, and it shows clearly that larger D produces more accurate results, and in the large- D limit, a power-law extrapolation gives a very consistent critical field, $h_c = 3.0445$.

Regarding the critical exponent in the relaxation process, it shows that although the estimated critical field h^* depends sensitively on D , the extracted exponents remain remarkably consistent across all cases. The proximity of the fitted slopes k^* to the previous estimation $-\beta/(\nu z) \approx -0.518$ [10] demonstrates the fact that the critical scaling behavior of short-time magnetization decay can be reliably captured, even at modest bond dimensions. The discrepancy in the critical field arises primarily from finite- D effects, which cause a systematic overestimation of h_c at smaller D . However, once scaling behavior is observed, the slope itself serves as a robust observable for benchmarking dynamical universality.

As a summary of this section, by using the iPEPS

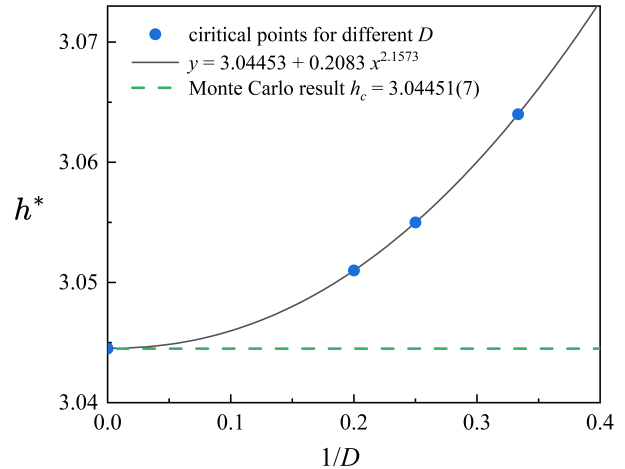


FIG. 2: Extrapolation of the estimated critical field h^* as a function of $1/D$. The data points correspond to the result obtained from $D = 3, 4$, and 5 , which are determined from the best power-law fitting. A simple power fit yields an extrapolated value of $h_c \approx 3.0445$, in close agreement with the previous estimation $h_c = 3.04451(7)$ [10] (denoted as green dashed line).

method with the full-update strategy, we demonstrate that the imaginary-time relaxation dynamics of magnetization at the critical point exhibits robust power-law decay consistent with universal scaling theory. Despite shifts in the estimated critical field due to finite- D effect, the extracted exponent $-\beta/(\nu z)$ remains remarkably stable and close to the previous estimations. This confirms that once proper scaling behavior is observed,

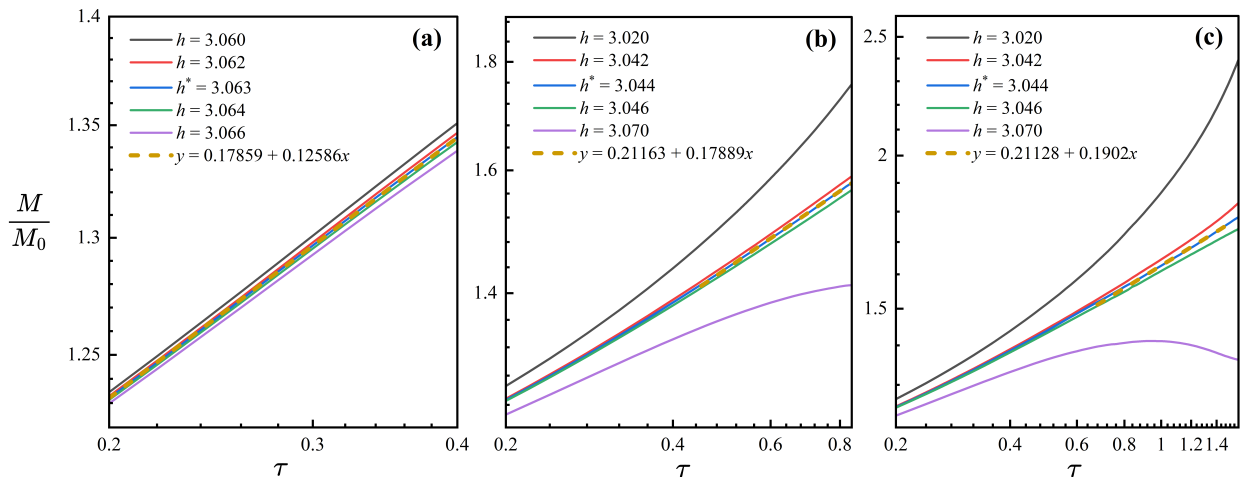


FIG. 3: Imaginary-time relaxation dynamics for a product initial state with a tiny magnetization $M_0 \approx 0.005$, plotted in log-log scale. Magnetization $M(\tau)/M_0$ obtained from iPEPS with different bond dimensions (D) and environment bond dimensions (χ) is summarized together. In each calculation, the transverse field leading to the best linear curve is denoted as h^* , and for each h^* a linear fitting is performed and is denoted as dashed yellow. (a) For $D = 3$ and $\chi = 30$. (b) For $D = 4$ and $\chi = 60$. (c) For $D = 5$ and $\chi = 60$.

the exponent can serve as a reliable and accurate probe of dynamical universality. Moreover, finite- D extrapolation provides a controlled pathway to refine critical point estimates in tensor network simulations of quantum dynamics.

B. Relaxation dynamics for a product state with small magnetization

In this section, in order to reveal the critical initial-slip behavior [8, 9, 12–15] characterized by Eq. (4), starting from an uncorrelated state with a tiny magnetization, we investigate the short-time critical dynamics of TFIM. Similarly, we have done a series of calculations with different setups of D and χ , and the results are summarized in Fig. 3.

Similar to the discussion in the last section, at the critical point in this case, the magnetization should exhibit a power behavior $M(\tau) \sim \tau^\theta$ as expressed in Eq. (4) and Eq. (5). Therefore, to guide the eyes, we plot Fig. 3 on a log-log scale too. Moreover, following the same procedure, we determine a h^* leading to the best power behavior of $M(\tau)$ for each (D, χ) setup, and use it as an approximate estimator of the critical transverse field h_c . The critical initial-slip exponent can be extracted by performing a power-law fitting at $h = h^*$, as denoted also by dashed yellow lines in Fig. 3.

As shown in Fig. 3(a), for $D = 3$, we find $h^* = 3.063$ and the best power-law fitting in the range $0.2 < \tau < 0.5$ gives a slope $k^* = 0.12586$. Increasing to $D = 4$, Fig. 3 shows a more pronounced power-law scaling behavior in the range $0.5 < \tau < 0.84$ at $h^* = 3.044$, which is much closer to the known critical value. The fitted exponent is

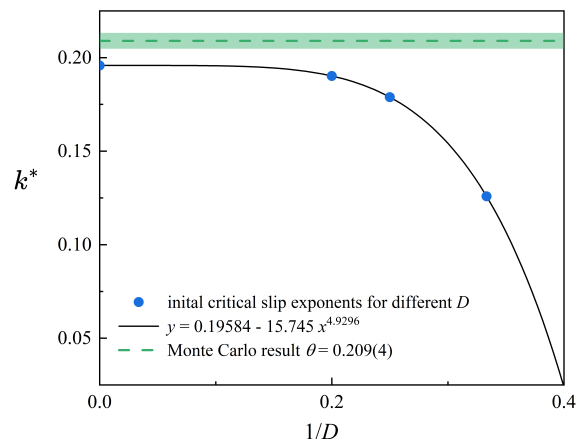


FIG. 4: The fitting power at $h = h^*$ as a function of $1/D$. The data points correspond to $D = 3, 4$, and 5 , with critical fields determined from the best power-law fits in Fig. 3. A simple power-law fit yields $\theta \approx 0.19584$ in the large- D limit, consistent with the QMC estimation $0.209(4)$ [10] denoted by the green dashed line with the shaded area indicating the statistical error.

$k^* = 0.17889$, which is also closer to the value $0.209(4)$ obtained from a previous Monte Carlo simulation [10]. This improvement highlights again the enhanced ability of the iPEPS ansatz to capture critical correlation growth at larger D . Moreover, it is clear that when h deviates from the approximate critical field h^* , the $M(\tau)$ curves deviate obviously from the power behavior in the short-time stage. This critical behavior is more manifestly shown in Fig. 3(c) with $D = 5$, $h^* = 3.044$ and $k^* = 0.1902$, where it shows clearly that the magnetiza-

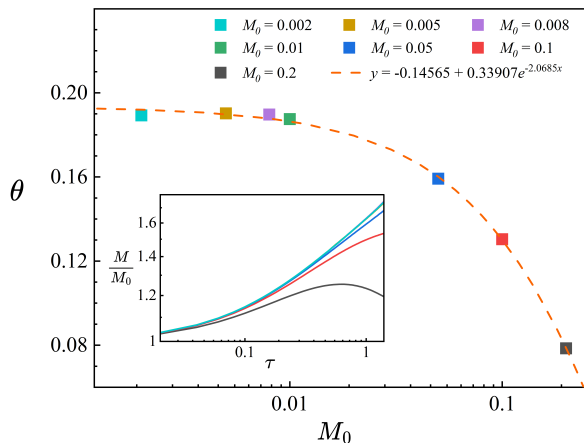


FIG. 5: Estimated critical initial-slip exponent k^* as a function of initial magnetization M_0 , obtained with $D = 5$ and $\chi = 60$. Each data point is obtained at $h^* = 3.044$ as shown in Fig. 3 and discussed in the main text. An exponential fit is performed and is denoted by the orange dashed line. Inset: the initial-slip behavior of magnetization as a function of τ when M_0 is small.

tion curve bends upward when $h < h^*$ and bends downward obviously when $h > h^*$.

Moreover, in order to give a more accurate critical initial-slip exponent θ , Fig. 4 presents a power-law fitting of k^* as a function of $1/D$, using the values extracted from Fig. 3. The extrapolated value in the large- D limit gives $\theta = 0.19584$, which agrees well with the quantum Monte Carlo estimation $0.209(4)$ [10]. This confirms that increasing the bond dimension enables iPEPS to refine the universal short-time quantum critical dynamics further.

In this work, we use an initial state with $M_0 = 0.005$ to simulate the relaxation dynamics. However, it should be noticed that the scaling behavior of short-time critical initial-slip, i.e., Eq. (4), requires a nearly paramagnetic initial state with a sufficiently small M_0 in order to guarantee the leading Taylor expansion in Eq. (3) a good approximation. To check this, in Fig. 5, we preform the calculations for several initial state with different M_0 . In the inset of Fig. 5, it shows that when $M_0 \lesssim 0.1$, M indeed grows following the power law after some transient time, reflecting the critical initial-slip behavior. Moreover, from the behavior of the estimated exponent θ as a function of M_0 , it also shows that as M_0 becomes smaller, the data match with each other, confirming the onset of universal behavior $M \propto \tau^\theta$. In the small- M_0 limit, we obtain an exponent $\theta = 0.19342$ by extrapolating an exponential fitting to the limit of $M_0 = 0$, which is in good agreement with previous predictions for the 2D TFIM universality class [10].

V. CONCLUSIONS AND OUTLOOK

In this work, we have investigated the imaginary-time relaxation dynamics of the two-dimensional TFIM using the full-update-assisted iPEPS method. By calculating the order parameter as a function of imaginary-time from two distinct initial states respectively as an initial state, i.e., a fully polarized state with $M_0 = 1$ and a product state with $M_0 = 0.005$, we have found rich critical dynamical behaviors in universal short-time stages.

For the saturated initial state, we observed an algebraic decay of the magnetization $M(\tau) \sim \tau^{-\beta/(\nu z)}$ [8, 9]. By fitting the log-log slope of the magnetization curve at various transverse fields, we not only determined the critical field h_c but also extracted the critical exponent $-\beta/(\nu z)$. The obtained exponent remained close to the expected universal value -0.518 [10] for all tested bond dimensions, and at the same time, the estimated critical field showed systematic drift depending on D due to finite-entanglement effects. Extrapolation of the critical point to the large- D limit yielded $h_c \approx 3.0445$, in excellent agreement with the known value 3.044 [40, 41, 45].

We also examined the critical initial-slip behavior starting from a nearly paramagnetic state with a tiny magnetization ($M_0 = 0.005$). Simulations with increasing bond dimensions show systematic improvement in the extracted exponent θ , and extrapolation to the large- D limit yields $\theta \approx 0.19584$, consistent with the QMC estimation $\theta_{\text{QMC}} \approx 0.209(4)$ [10]. This confirms that iPEPS can reliably capture universal short-time dynamics with moderate bond dimensions.

Overall, our results establish the imaginary-time iPEPS algorithm as a powerful and accurate tool for probing critical quantum dynamics in two dimensions. In the short-time stage, both critical point and critical exponents can reliably be extracted. Future directions include improving initial state preparation via variational methods or imaginary-time annealing to reduce finite-entanglement artifacts, and extending this framework to frustrated or sign-problematic systems beyond the reach of quantum Monte Carlo, to open a path to studying non-equilibrium criticality in broader classes of quantum matter.

ACKNOWLEDGMENTS

Computational resources used in this study were provided by the National Supercomputer Center in Guangzhou with Tianhe-2 Supercomputer and the Physical Laboratory of High-Performance Computing in Renmin University of China. This work was supported by the National R&D Program of China (Grants No. 2024YFA1408600, 2023YFA1406500), the National Natural Science Foundation of China (Grants No. 12434009 and Grants No. 12274458), and the Innovation Program for Quantum Science and Technology (2021ZD0302402). S.Y. is supported by the

National Natural Science Foundation of China (Grant No. 12222515), the Research Center for Magneto-electric Physics of Guangdong Province (Grant No. 2024B0303390001), and the Guangdong Provincial Key Laboratory of Magnetolectric Physics and Devices

(Grant No. 2022B1212010008). S.Y. is also supported by the Science and Technology Projects in Guangdong Province (Grant No. 2021QN02X561) and Guangzhou City (Grant No. 2025A04J5408). H.-Y.L and S.Y. contributed equally to this work.

-
- [1] G. Vidal, Phys. Rev. Lett. **91**, 147902 (2003); G. Vidal, Phys. Rev. Lett. **93**, 040502 (2004); G. Vidal, Phys. Rev. Lett. **98**, 070201 (2007).
- [2] H. C. Jiang, Z. Y. Weng, and T. Xiang, Phys. Rev. Lett. **101**, 090603 (2008).
- [3] P. Corboz, T. M. Rice, and M. Troyer, Phys. Rev. Lett. **113**, 046402 (2014); P. Corboz, Phys. Rev. B **93**, 045116 (2016).
- [4] Z. Y. Xie, J. Chen, J. F. Yu, X. Kong, B. Normand, and T. Xiang, Phys. Rev. X **4**, 011025 (2014).
- [5] W. X. Chang, S. Yin, S. X. Zhang, and Z. X. Li, arXiv:2409.06547 (2024).
- [6] M. Motta, C. Sun, A. T. K. Tan, M. J. O'Rourke, E. Ye, A. J. Minnich, F. G. S. L. Brandão, and G. Kin-Lic Chan, Nature Phys. **16**, 205 (2020).
- [7] T. Tsuchimochi, Y. Ryo, S. L. Ten-no, and K. Sasasako, npj Quantum Inf. **7**, 85 (2021).
- [8] S. Yin, P. Mai, and F. Zhong, Phys. Rev. B **89**, 144115 (2014).
- [9] S. Zhang, S. Yin, and F. Zhong, Phys. Rev. E **90**, 042104 (2014).
- [10] Y.-R. Shu, S. Yin, and D.-X. Yao, Phys. Rev. B **96**, 094304 (2017).
- [11] Z.-X. Li, S. Yin, and Y.-R. Shu, Chin. Phys. Lett. **40**, 037501 (2023).
- [12] H. K. Janssen, B. Schaub, and B. Schmittmann, Z. Phys. B **73**, 539 (1989).
- [13] Z. B. Li, L. Schülke, and B. Zheng, Phys. Rev. Lett. **74**, 3396 (1995).
- [14] B. Zheng, Phys. Rev. Lett. **77**, 679 (1996).
- [15] B. Zheng, Int. J. Mod. Phys. B **12**, 1419 (1998).
- [16] Y.-R. Shu, S.-K. Jian, and S. Yin, Phys. Rev. Lett. **128**, 020601 (2022).
- [17] Y.-R. Shu and S. Yin, Phys. Rev. B **105**, 104420 (2022).
- [18] Y. K. Yu, Z. X. Li, S. Yin, and Z. X. Li, arXiv:2410.18854 (2024).
- [19] Y. K. Yu, Z. Zeng, Y. R. Shu, Z. X. Li and S. Yin, arXiv:2310.10601 (2023).
- [20] S.-X. Zhang and S. Yin, Phys. Rev. B **109**, 134309 (2024).
- [21] A. Avella, F. Mancini, *Strongly Correlated Systems, Numerical Methods*, Springer (2013).
- [22] T. Xiang, *Density Matrix and Tensor Network Renormalization*, Cambridge (2023).
- [23] J. Eisert, M. Cramer, and M. B. Plenio, Rev. Mod. Phys. **82**, 277 (2010).
- [24] P. Corboz and F. Mila, Phys. Rev. B **87**, 115144 (2013); P. Corboz and F. Mila, Phys. Rev. Lett. **112**, 147203 (2014).
- [25] H. J. Liao, Z. Y. Xie, J. Chen, Z. Y. Liu, H. D. Xie, R. Z. Huang, B. Normand, and T. Xiang, Phys. Rev. Lett. **118**, 137202 (2017).
- [26] Q. Li, H. Li, J. Z. Zhao, H. G. Luo, and Z. Y. Xie, Phys. Rev. B **105**, 184418 (2022).
- [27] Ning Xi, Hongyu Chen, Z. Y. Xie, and Rong Yu, Phys. Rev. B **107**, L220408 (2023).
- [28] He-Yu Lin, Yibin Guo, Rong-Qiang He, Z. Y. Xie, Zhong-Yi Lu, Phys. Rev. B **109**, 235133 (2024).
- [29] Z. T. Xu, Z. C. Gu, and S. Yang, Phys. Rev. B **108**, 035144 (2023).
- [30] J. W. Mei, J. Y. Chen, H. He, and X. G. Wen, Phys. Rev. B **95**, 235107 (2017).
- [31] Y. H. Chen, K. Hsu, W. L. Tu, H. Y. Lee, and Ying-Jer Kao, Phys. Rev. Research **4**, 043153 (2022).
- [32] Rui Wang, Z. Y. Xie, Baigeng Wang, Tigran Sedrakyan, Phys. Rev. B **106**, L121117 (2022); Rui Wang, Tao Yang, Z. Y. Xie, Baigeng Wang, X. C. Xie, Phys. Rev. B **109**, L241113 (2024).
- [33] F. Verstraete and J. I. Cirac, Phys. Rev. Lett. **104**, 190405 (2010).
- [34] A. Tilloy and J. I. Cirac, Phys. Rev. X **9**, 021040 (2019).
- [35] F. Verstraete, and J. I. Cirac, arXiv:cond-mat/0407066.
- [36] J. Jordan, R. Orus, G. Vidal, F. Verstraete, and J. I. Cirac, Phys. Rev. Lett. **101**, 250602 (2008).
- [37] M. Lubasch, J. I. Cirac, and M. C. Banuls, Phys. Rev. B **90**, 064425 (2014).
- [38] Ho N. Phien, Johann A. Bengua, Hoang D. Tuan, Philippe Corboz, Roman Orus, Phys. Rev. B **92**, 035142 (2015).
- [39] P. Pfeuty, Ann. Phys. **57**, 79 (1970).
- [40] H. Rieger and N. Kawashima, Eur. Phys. J. B **9**, 233 (1999).
- [41] H. W. J. Blöte and Y. Deng, Phys. Rev. E **66**, 066110 (2002).
- [42] S. Sachdev, *Quantum Phase Transitions*, 2nd ed., Cambridge University Press (2011).
- [43] A. Dutta, G. Aeppli, B. K. Chakrabarti, U. Divakaran, T. F. Rosenbaum, and D. Sen, *Quantum Phase Transitions in Transverse Field Spin Models: From Statistical Physics to Quantum Information*, Cambridge University Press (2015).
- [44] J. Dziarmaga, Phys. Rev. Lett. **95**, 245701 (2005).
- [45] Z. Y. Xie, J. Chen, M. P. Qin, J. W. Zhu, L. P. Yang, and T. Xiang, Phys. Rev. B **86**, 045139 (2012).
- [46] B. K. Chakrabarti, A. Dutta, and P. Sen, *Quantum Ising Phases and Transitions in Transverse Ising Models*, Springer-Verlag (1996).
- [47] M. Suzuki, Prog. Theor. Phys. **56**, 1454 (1976).
- [48] J. I. Cirac, D. Perez-Garcia, N. Schuch, and F. Verstraete, arXiv.2011.12127.
- [49] L. Vanderstraeten, M. Marien, F. Verstraete, and J. Haegeman, Phys. Rev. B **92**, 201111(R) (2015).
- [50] B. Ponsioen, F. F. Assaad, and P. Corboz, SciPost Phys. **12**, 006 (2022).
- [51] B. B. Chen, L. Chen, Z. Chen, W. Li, and A. Weichselbaum, Phys. Rev. X **8**, 031082 (2018).
- [52] Q. Yi, Y. Gao, Y. He, Y. Qi, B. B. Chen, and W. Li, Phys. Rev. Lett. **130**, 226502 (2023).

- [53] J. W. Li, A. Gleis, and J. von Delft, Phys. Rev. Lett. **133**, 026401 (2024).
- [54] P. Czarnik, J. Dziarmaga, and P. Corboz, Phys. Rev. B **99**, 035115 (2019).
- [55] R. Orús and G. Vidal, Phys. Rev. B **80**, 094403 (2009).